

Multi-objective optimization design of a heavy-duty folding mechanism and Self-discharging equipment development

Juan Huang^{1,2}, Chongxiang Li³, Huang Long^{*,2}, Lairong Yin², Bo Wen², and Jinhang Wang²

¹ College of Mechanical and Electrical Engineering, Hunan Agriculture University, Changsha 410128, China

² School of Automotive and Mechanical Engineering, Changsha University of Science and Technology, Changsha 410114, China

³ School of Mechanical Engineering, University of Science and Technology Beijing, Beijing 100083, China

Received: 6 April 2022 / Accepted: 18 April 2023

Abstract. In this paper, we investigated the technical problem of the recovery of overlength and heavy load conveying booms of self-unloading ships. A method of folding the conveying boom with a hydraulic-four-bar mechanism is presented, and by using a mathematical model for the optimization of folding velocity stationary with ADAMS software, the optimization data and results were obtained. The multi-objective optimization index is introduced, and the multi-objective optimization problem is discussed. The results of the multi-objective optimization showed that parameters such as angular velocity and the change of angular acceleration of the conveyor boom were optimized. The paper has manufactured the connecting rod mechanism, and developed the self-discharging folding conveyance equipment. Through practical application, we determined that the developed folding conveying equipment had the advantages of smooth movement and high folding efficiency.

Keywords: Four-bar linkage / optimization design / kinematic analysis / equipment development

1 Introduction

The traditional self-unloading sand-ship often uses a fixed overhanging boom to unload sand. The key technical problems with this, such as the large size, unreturnable belt frame and poor safety, need to be solved urgently. To solve these problems, researchers have obtained a series of results, which have been summed into four solutions: telescopic, rotary, folding and flip. Among them, the folding boom recovery scheme was first proposed in [1], which uses the hydraulic-four-bar folding mechanism to realize the folding recovery of a 43.8-meter two-section boom (also the object of this paper). The comprehensive theory of linkage mechanisms and multi-objective optimization design have been classical research focuses in the field of mechanical design. Optimization design has been widely studied in optimization theory, mechanical properties, and material manufacturing [2–5]. Hassan et al. [6] used the non-dominated sorting genetic algorithm version II (NSGA-II) to optimize the robot gripper design. Qiu et al. [7] provided a simple design program to optimize the design of truss beams. Yalcin et al. [8] introduced an improved optimization algorithm, which can quickly obtain the scheme of Mechanically Stabilized Earth Walls (MSEW). Rao et al. [9] proposed Rao algorithms and

discussed the performance of Rao algorithms in the optimization of mechanical system parts design. Bai et al. [10] proposed a design optimization method for satellite antenna that takes into account the gap node of a biaxial drive mechanism, and used the generalized reduced gradient (GRG) algorithm to significantly reduce the peak acceleration of the satellite antenna and the contact force of the gap node. Cicero et al. [11] adopted the method of topology optimization to optimize the design of the compliant mechanism, and solved the problem of hinges (single-node connections) in the design of the flexible mechanism. Wang et al. [12] presented an optimal design method to optimize a novel subsea pipeline mechanical connector. Ma et al. [13] optimized the bed structure of the gantry-type machining center presented by using a lightweight design method. The solution-region method can be used to optimize the linkage mechanism [14,15], and there are still many cases where kinematics requirements need to be considered [16–18]. Gabardi et al. [19] conducted the kinematic analysis of the 4-UPU fully parallel manipulator to maximize the performance parameters in the design workspace. Nisar et al. [20] proposed a new remote center of motion (RCM) mechanism design for minimally invasive surgery (MIS) robotic manipulators, and optimized and reduced the size of the mechanism. Russo et al. [21] optimized the parallel mechanism with 3-UPR architecture for a robotic leg application by using four different objective functions. Hu et al. [22,23] proposed

* e-mail: huanglongjin@foxmail.com

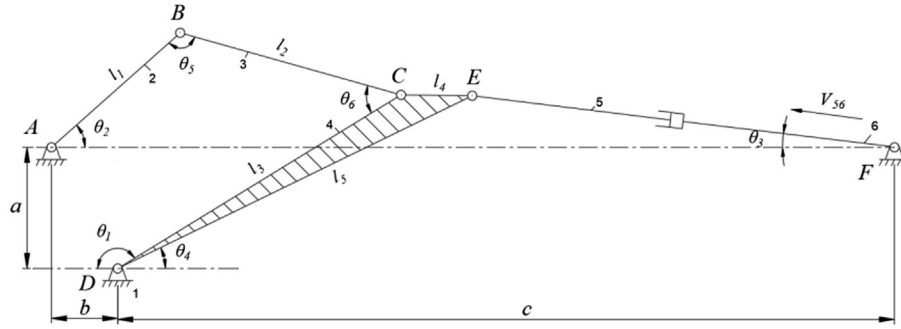


Fig. 1. Schematic diagram of four-bar mechanism motion.

a method for the prediction and validation of dynamic characteristics of a valve train system with flexible components and gyroscopic effects.

To solve the problem of self-unloading sand-ship super-long overloading transportation boom recovery, this paper proposes a hydraulic, folding transportation boom of the four-bar linkage. The mathematical model for folding velocity stability, the hydraulic oil cylinder force optimization problem, and the multi-objective optimization problem are discussed, and a self-unloading sand-ship conveying equipment is developed.

2 Mathematical modeling of the optimization of the four-bar mechanism

2.1 Design variables and constraints

Figure 1 shows the schematic diagram of a four-bar folding mechanism and the related dimensions of the research object. The state shown in the figure is the initial state of complete folding, V_{56} is the relative velocity of the original moving part 5 relative to component 6 (that is the propulsion velocity of the hydraulic cylinder). As shown in Figure 1, the folding arm (link 2) can flip 180° under the push of the hydraulic cylinder (links 5 and 6).

Design variables are defined as:

$$\begin{aligned} X &= \{x_1, x_2, x_3, x_4, x_5, x_6, x_7, x_8, x_9\}^T \\ &= \{a, b, l_1, l_3, l_5, \theta_1, \theta_2, \theta_3, \theta_4\}^T \end{aligned} \quad (1)$$

Consider that the folding arm can flip 180° ; the four-bar mechanism satisfies the bar length condition, and rotating pair B is the rotating pair. Set A - D as the shortest bar. According to the shortest bar condition and the bar length condition, the constraint conditions are as follows:

$$\overline{AD} \leq l_1, \overline{AD} \leq l_2, \overline{AD} \leq l_3, \quad (2)$$

$$\overline{AD} + l_1 \leq l_2 + l_3, \quad (3)$$

$$\overline{AD} + l_2 \leq l_1 + l_3, \quad (4)$$

$$\overline{AD} + l_3 \leq l_1 + l_2. \quad (5)$$

2.2 The objective function

Kinematic analysis is the basis of studying the dynamic characteristics of the mechanism. Figures 2 and 3 show the motion analysis diagram of the four-bar mechanism.

Through kinematic analysis and calculation, we deduced that the reversal angular velocity and angular acceleration of the folding arm were as follows:

$$\omega_2(X) = \frac{l_3 V_{56} \sin \theta_6}{l_1 l_5 \sin(\theta_3 + \theta_4) \sin \theta_5}, \quad (6)$$

$$\alpha_2 = \frac{\alpha_4 l_3 \sin \theta_6 + \omega_4^2 l_3 \cos \theta_6 - \omega_3^2 l_2 + \omega_2^2 l_1 \cos \theta_5}{l_1 \sin \theta_5}. \quad (7)$$

Among them

$$\theta_5 = \arccos \frac{l_1 + l_3 \cos(\theta_1 + \theta_2) - b \cos \theta_2 + a \sin \theta_2}{l_2}, \quad (8)$$

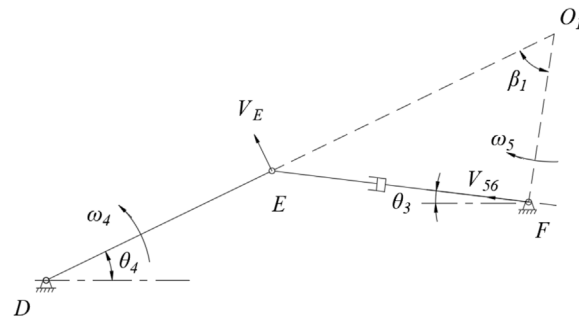
$$\theta_6 = \arccos \frac{l_3 + l_1 \cos(\theta_1 + \theta_2) - b \cos \theta_1 - a \sin \theta_1}{l_2}, \quad (9)$$

$$l_2 = \sqrt{(-l_3 \cos \theta_1 - l_1 \cos \theta_2 + b)^2 + (l_3 \sin \theta_1 - a - l_1 \sin \theta_2)^2}, \quad (10)$$

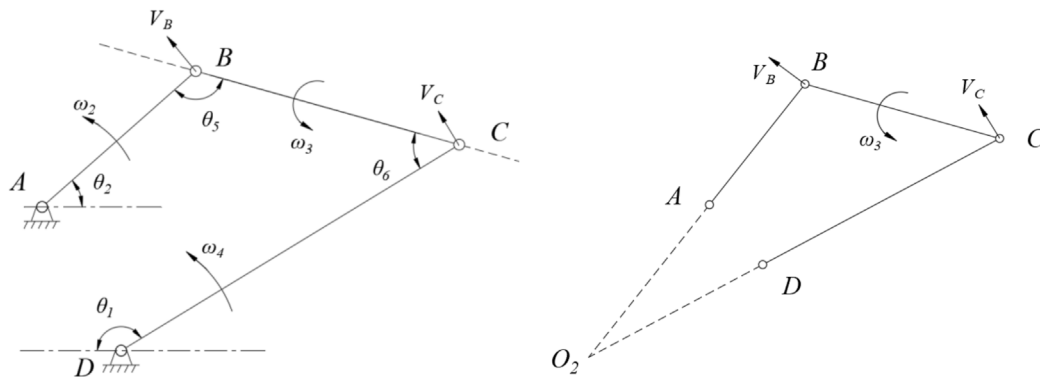
$$\omega_3 = \frac{l_3 V_{56} \sin(\theta_5 + \theta_6)}{l_2 l_5 \sin(\theta_3 + \theta_4) \sin \theta_5}, \quad (11)$$

$$\omega_4 = \frac{V_{56}}{l_5 \sin(\theta_3 + \theta_4)}, \quad (12)$$

$$\omega_5 = \frac{V_{56} \sin \theta_3}{\tan(\theta_3 + \theta_4) \cdot (l_5 \sin \theta_4 - a)}, \quad (13)$$

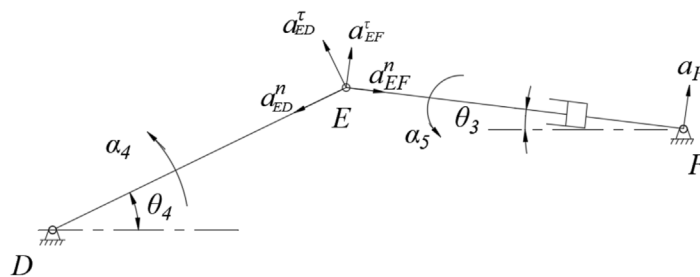


(a) Velocity analysis diagram of the hydraulic rod.

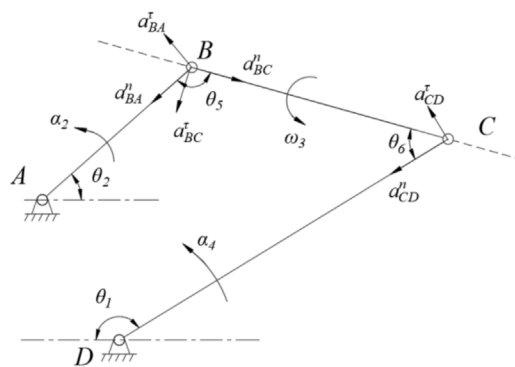


(b) Velocity analysis diagram of the four-bar mechanism.

Fig. 2. Velocity analysis diagram of four-bar mechanism.

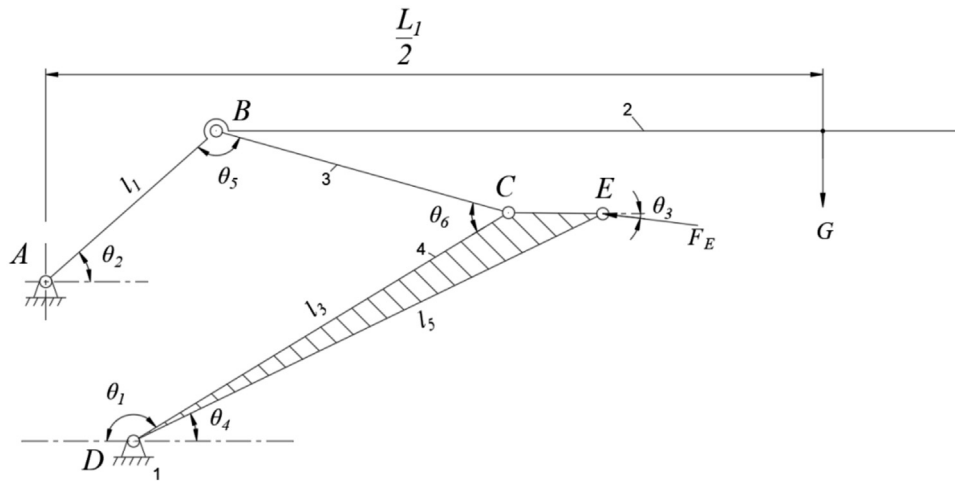


(a) Acceleration analysis diagram of hydraulic rod

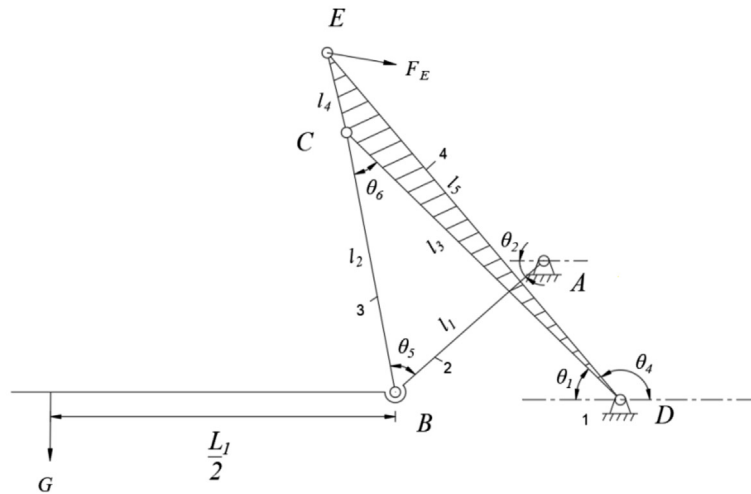


(b) Acceleration analysis diagram of the four-bar mechanism

Fig. 3. Acceleration analysis diagram of the four-bar mechanism.



(a) Diagram of force analysis in the state of just pushing.



(b) Diagram of force analysis in the just-pulled state

1-Frame; 2-Folding arm; 3-The two connecting rod; 4-The three articulated connecting rod

Fig. 4. Force analysis diagram of the four-bar linkage.

$$V_E = \omega_5 \cdot E - O_1 = \frac{V_{56}}{\sin(\theta_3 + \theta_4)}, \tag{14}$$

$$\overline{EF} = \frac{l_5 \sin \theta_4 - a}{\sin \theta_3}, \tag{15}$$

$$\alpha_4 = -\frac{\omega_5^2 l_5 \overline{EF} + V_E^2 \cos(\theta_3 + \theta_4)}{l_5^2 \sin(\theta_3 + \theta_4)}. \tag{16}$$

When working, the rotation velocity of the folding arm was stable. By optimizing the maximum value of angular acceleration, the stability of the velocity was optimized indirectly. The objective function of the angular velocity stability of the folding arm was as follows:

$$F_1(X) = \min[\max \alpha_2(X)]. \tag{17}$$

In addition to the stability of the turning angular velocity, the force condition of the hydraulic cylinder was considered. The maximum thrust force of the hydraulic cylinder determined the diameter, which therefore affected the manufacture of the mechanism. Currently, when the complete folding state was about to be expanded, the hydraulic cylinder received a maximum thrust.

The force analysis diagram of the connecting rod mechanism is shown in Figure 4. The thrust of the hydraulic cylinder is F_E , the folding arm weight is G , and the total length of the folding arm is L_J . Through force analysis and calculation, the thrust (or tension) of the hydraulic cylinder could be obtained as follows:

$$F_E(X) = \frac{GL_1 l_3 \sin \theta_6}{2l_1 l_5 \sin \theta_5 \sin(\theta_3 + \theta_4)}. \tag{18}$$

Table 1. Initial dimensions of the four-bar linkage.

Structure size	a	b	c	l_1	l_2	l_3	l_4	l_5
The initial value/mm	400	220	3885	570	760	1100	236	1300

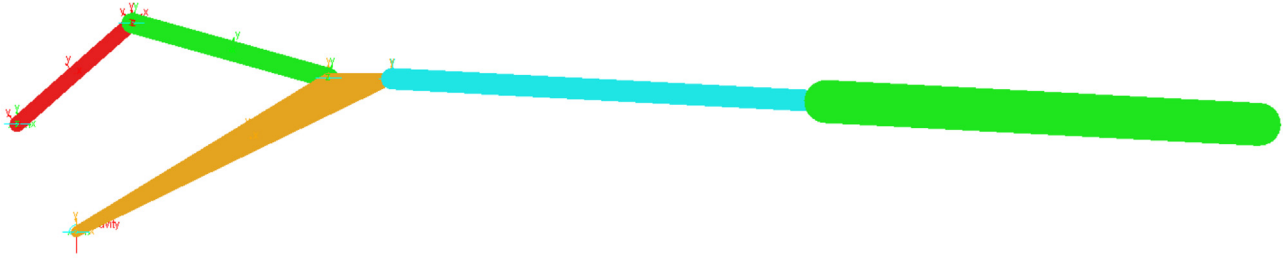


Fig. 5. ADAMS model of the four-bar linkage.

In the process of flipping, the gravity direction was unchanged, so equation (18) needed to be multiplied by the coefficients of $\cos(\theta_2 + \theta_2')$ and θ_2' to make the value of $\theta_2 + \theta_2'$ equal to 0. Then equation (19) could be used to represent the force formula of the hydraulic cylinder in the whole folding process. When its value was regular, it was thrust, and when it was negative, it was tension.

$$F_E(X) = \frac{GL_1 l_3 \sin \theta_6 \cos(\theta_2 + \theta_2')}{2l_1 l_5 \sin \theta_5 \sin(\theta_3 + \theta_4)}. \quad (19)$$

In practical engineering, the smaller the maximum pressure required for the thrust and tension of the hydraulic cylinder, the more economical the hydraulic cylinder. Suppose the pressure required for the thrust was P_1 , the pressure required for tension was P_2 , and the maximum pressure required for hydraulic cylinder expansion and folding was P_{\max} . The difference between the pressure required for the maximum thrust and the pressure required for the maximum tension was P , the diameter of the hydraulic cylinder was D , and the diameter of the rod was d . According to equation (19), the following could be obtained:

$$P_1 = \frac{4F_{E1}}{\pi D^2}, \quad (20)$$

$$P_2 = \frac{4F_{E2}}{\pi(D^2 - d^2)}, \quad (21)$$

$$P = |P_{1\max} - P_{2\max}|, \quad (22)$$

$$P_{\max} = \max\{p_{1\max}, p_{2\max}\}. \quad (23)$$

Thus, the objective function for the force optimization of the hydraulic cylinder in the four-bar linkage was as follows:

$$F_2(X) = \min P_{\max}. \quad (24)$$

3 Optimal design for velocity stationarity

According to the optimization model for the angular velocity stability of a four-bar mechanism, we could get the optimization result of the velocity stability. However, in the actual optimization design process, too many design variables and objective functions made it difficult to express the optimization and derive the optimization result. Therefore, we used the complex method embedded in ADAMS software to optimize the velocity stationarity of the four-bar linkage. The initial calculation size of the four-link mechanism is shown in Table 1, and its parametric model is shown in Figure 5.

Nine design variable transformations for points A, B, C, D, E, F with 10 initial coordinate variables (folding arm folded state) were used with maximum angular acceleration as the optimization target. Reducing the maximum angular acceleration made four bar-linkage flip angular velocity stability optimized, and the sensitivity analysis of the 10 coordinate variables on the angular acceleration is carried out. The results are shown in Table 2.

In Table 2, it can be found how much each design variable influences the folding velocity at its initial value, and the sensitivity of y_A, y_B, y_E to the folding velocity was highest. Therefore, y_A, y_B, y_E were selected as the key design variables, and equation (17) was used as the optimization objective function for optimization analysis. The optimization analysis results are shown in Table 3.

Table 2. Design variables and sensitivity analysis results of the four-bar linkage.

Design variables	Design point	Coordinate direction	Initial value	Sensitivity to initial values/deg · s ⁻² · m ⁻¹
x_A	POINT_A	X	-220	14.72
y_A	POINT_A	Y	400	374.58
x_B	POINT_B	X	207.2	-5.63
y_B	POINT_B	Y	777.3	376.65
x_C	POINT_C	X	939.2	25.87
y_B	POINT_C	Y	572.7	170.89
x_E	POINT_E	X	1175.1	65.46
y_E	POINT_E	Y	569.8	880.28
x_F	POINT_F	X	4405	2.54
y_F	POINT_F	Y	400	168.65

Table 3. Optimization analysis results.

	Initial value	Range	Optimal value
y_A	400	300,500	300
y_B	777.3	677,877	877
y_E	569.8	470,870	670.1
Maximum angular acceleration/deg · s ⁻²	9.78		3.49

Table 3 shows that after optimization, the maximum angular acceleration of the folding arm was reduced by 64.4% in the folding process, and the stability of the folding velocity of the folding arm was optimized. To represent the optimization results of folding velocity stationarity of the folding arm, the comparison diagram of folding angular velocity and angular acceleration of the folding arm before and after the optimization was introduced, as shown in Figures 6 and 7. As can be seen from Figures 6 and 7, both the folding angular velocity and the maximum folding angular acceleration of the folding arm decreased significantly after optimization, and the folding velocity stationarity of the folding arm was optimized.

4 Multi-objective optimization design of a four-bar mechanism

4.1 Multi-objective optimization design for velocity stationarity

By referring to the unified objective function for the optimization design, an optimization index K was constructed to measure the effect of the multi-objective optimization results. The expression was as follows:

$$K = n_1 \frac{F_1(X)}{F_1(X_0)} + n_2 \frac{F_2(X)}{F_2(X_0)} + \dots + n_i \frac{F_i(X)}{F_i(X_0)}. \quad (25)$$

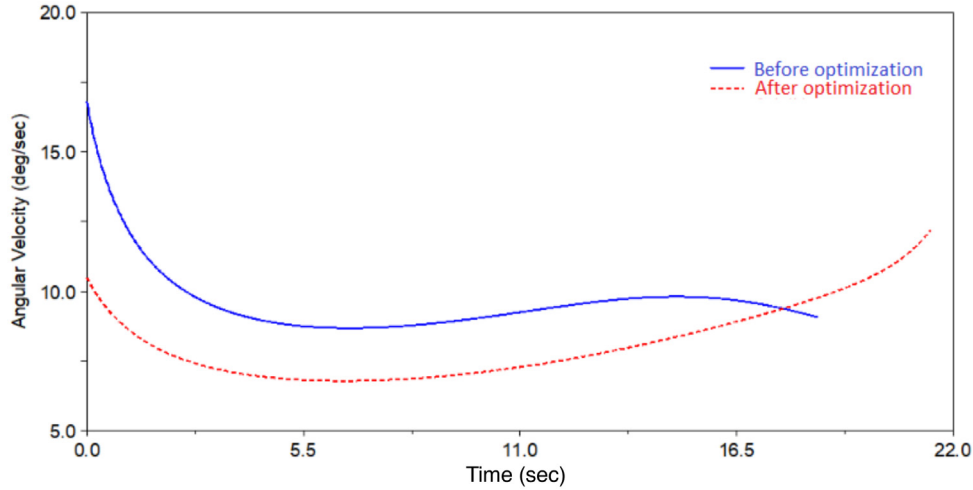


Fig. 6. The angular velocity curves of folding arms before and after optimization.

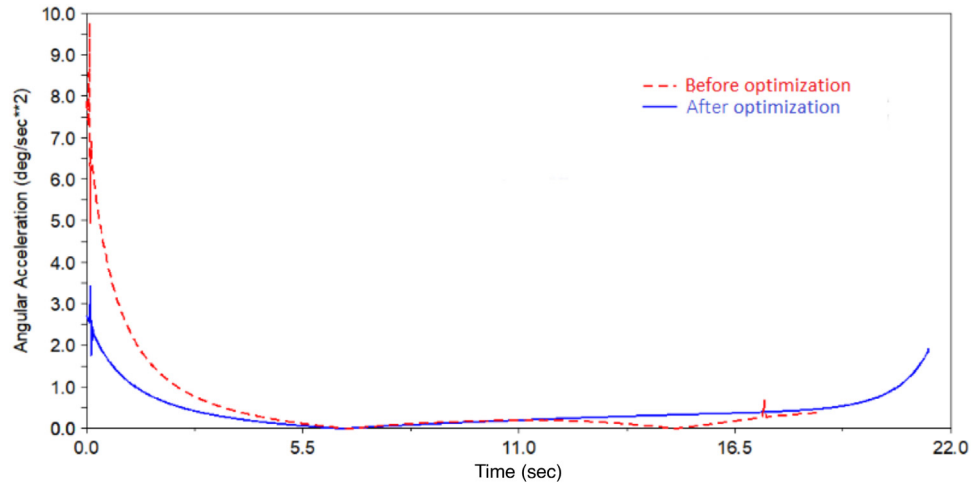


Fig. 7. The angular acceleration curves of folding arms before and after optimization.

Table 4. The value of the weight factor and the initial value of the related angular velocity.

	ω_{0f} (deg/s)	ω_{0max} (deg/s)	ω_{0min} (deg/s)	n_1	n_2	n_3
Initial value	9.11	16.8	8.71	0.39	0.16	0.45

$F_i(X)$ were the objective functions, $F_i(X_0)$ were the initial values of each objective function, n_i was the weight factor, and $n_1 + n_2 + \dots + n_i = 1$.

Using the optimization index K and simulation data, the optimization performance was calibrated more comprehensively. The expression for the velocity stationarity optimization index K was as follows:

$$K_1 = n_1 \frac{\omega_{0f}}{\omega_f} + n_2 \frac{\omega_{0max}}{\omega_{max}} + n_3 \frac{\omega_{0min}}{\omega_{0min}}, \quad (26)$$

ω_f was the angular velocity at the end of the folding arm expansion under different design variables, ω_{max} was the maximum angular velocity in the expansion process, ω_{min} was the minimum angular velocity in the expansion process, and ω_{0f} , ω_{0max} , and ω_{0min} were the corresponding initial values before optimization. The initial value and the weight factor are obtained through the `fmincon` function in MATLAB, as shown in Table 4.

By looking at the study on the diagonal acceleration sensitivity of the design variables in Table 2, it can be seen that the diagonal velocities of points y_E, y_A, y_B had a great

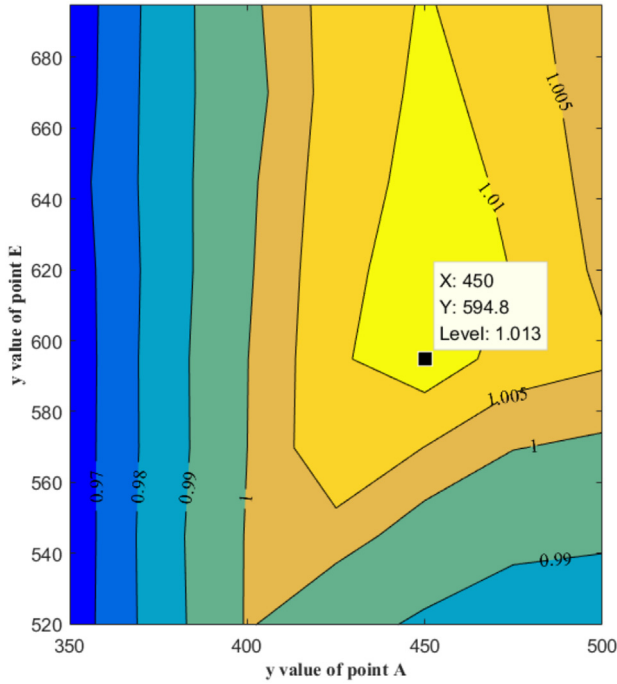


Fig. 8. Contour map of K_1 (y_E and y_A are variables).

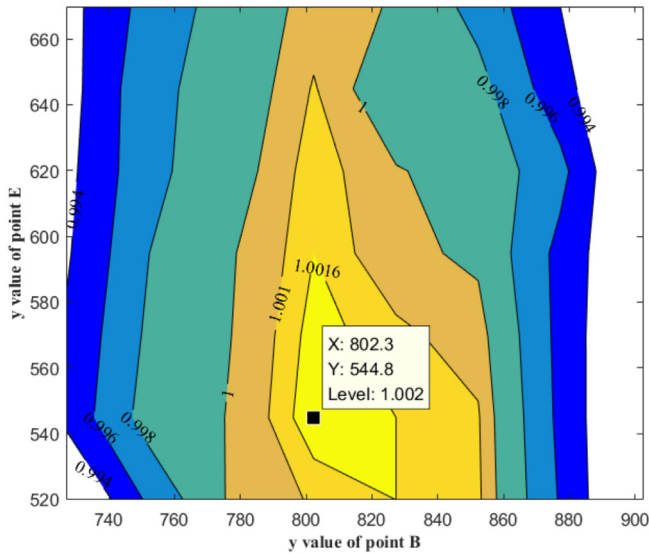


Fig. 9. Contour map of K_1 (y_E and y_B are variables).

influence; the influence of the three variables on the optimization index K_1 was mainly studied. The influence of y_E to y_A and y_B on the optimization index K_1 is shown in Figures 8 and 9.

According to Figures 8 and 9, we could not only obtain the optimal optimization solution under the relevant variables, but also found the relatively ideal optimization size data according to the corresponding optimization indexes. When point A was on the rack, the smaller the y_A value was, the more compact the overall structure was. The contour map of the influence of variables y_E and y_B on K_1 is shown in Figure 10. In Figure 10, we see that when

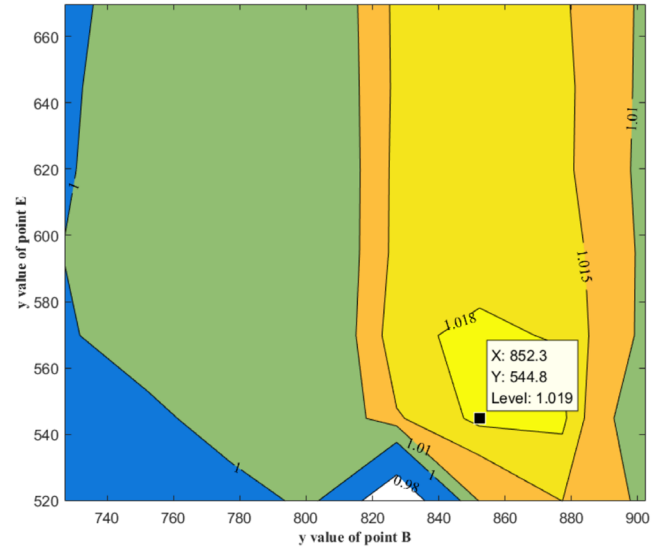


Fig. 10. Contour map of K_1 ($y_A=425$, y_E and y_B are variables).

$y_E = 544.8$ and $y_B = 852.3$, K_1 reached a maximum value of 1.019, and the optimal optimization results are shown in Table 5.

4.2 Multi-objective optimization design of a four-bar mechanism

The force on the hydraulic cylinder and the folding velocity multi-objective optimization index K_2 was expressed as follows:

$$K_2 = n_1 \frac{P_0}{P} + n_2 \frac{P_{0\max}}{P_{\max}} + n_3 \frac{\omega_0 f}{\omega_f} + n_4 \frac{\omega_{0\max}}{\omega_{\max}} + n_5 \frac{\omega_{\min}}{\omega_{0\min}}. \quad (27)$$

Values of the relevant data and weight factors of the hydraulic cylinder are shown in Table 6.

By equation (19), the maximum thrust or tension required for the hydraulic cylinder is in the starting or stopping position. Using Adams simulation data and equation (27), the value of optimization index K_2 can be obtained. The variables used were y_E and x_F , and y_A and y_B took the optimized values in Section 4.1 ($y_A=425$, $y_B=852.3$). When $y_E=519.8$ and $x_F=4255$, the maximum value of K_2 was 12.340, and the optimization results are shown in Table 7. In practice, the folding arm (link 2, in Fig. 4) did not reach the horizontal position; the actual pressure value is not actually at its maximum.

5 Prototype manufacturing and testing

Prototype manufacturing is divided into the 3D printing model and physical prototype. First, SolidWorks was used to conduct 3D modeling for each part of the connecting

Table 5. Optimization results of velocity stationarity.

	y_A	y_B	y_E	$l_1(\text{mm})$	$l_2(\text{mm})$	$l_4(\text{mm})$	$\omega_{\max} / \text{deg} \cdot \text{s}^{-1}$	$\omega_{\min} / \text{deg} \cdot \text{s}^{-1}$	$\omega_f / \text{deg} \cdot \text{s}^{-1}$
Initial value	400	777.3	569.8	570	760	236	16.80	8.71	9.09
Optimal value	425	852.3	544.8	604.2	783.6	237.5	16.66	8.80	8.82
Optimization percentage				6.00%	3.10%	0.65%	-0.83%	+1.03%	-2.97%

Table 6. Hydraulic cylinder related data and weight factor value.

	D	d	n_1	n_2	n_3	n_4	n_5
Initial value	200	140	0.2	0.2	0.2	0.2	0.2

Table 7. Multi-objective optimization results.

Coordinates size/mm	Initial value	Optimal value	Percentage of change	Optimization goal	Initial value	Optimal value	Optimization percentage
y_A	400	425	+6.25%	P/MPa	1.45	0.03	-97.93%
y_B	777.3	852.3	+9.65%	P_{\max}/MPa	25.16	24.85	-1.23%
y_E	569.8	519.8	-8.78%	$\omega_f/\text{deg} \cdot \text{s}^{-1}$	9.09	8.95	-1.57%
x_F	4405	4255	-3.41%	$\omega_{\max}/\text{deg} \cdot \text{s}^{-1}$	16.80	17.59	+4.70%
l_1	570	604.2	+6.00%	$\omega_{\min}/\text{deg} \cdot \text{s}^{-1}$	8.71	8.91	+2.30%
l_2	760	783.6	+3.10%				
l_4	236	241.8	+2.44%				
l_5	1305	1284.9	-1.54%				



(a) Model of four-bar mechanism (half-expanded state)



(b) Model of self-discharging transport equipment (fully expanded state)

Fig. 11. 3D printed model of the self-discharging equipment.



Fig. 12. Self-discharging equipment.

rod mechanism, and then the 3D model file was saved in the .stl format (the 3D model was automatically layered). This was converted to the printed program file in the software Cura.

The 3D Model of the four-bar mechanism is shown in Figure 11a. The folding arm can flip 180° under the push of the four-bar mechanism. As shown in Figure 11b, when the folding arm is fully expanded, the self-discharging transport equipment reaches the working state.

Through actual motion analysis of the 3D printed model, the parameters meet the expectations of the optimal design. Through cooperation with Hunan Xinghuo Machinery Manufacturing Co., the self-discharging transport equipment was manufactured, as shown in Figure 12. By using the special test platform, we see that the folding mechanism folding time was less than 12 minutes, and the maximum pressure of the hydraulic cylinder was less than 18 MPa, in line with the standards of transport equipment of self-discharging ships. The actual working test of the prototype showed that the folding time was the same as the pressure of the hydraulic cylinder, the conveying volume of the conveyor was the same as that of the traditional fixed conveyor, the conveying bandwidth was 1400 mm, and the conveying capacity was more than 4000 tons/hour, thus achieving all the expected functions.

6 Conclusion

In this paper, we aimed to solve the technical problem of recovery of overlength and heavy load conveying booms of self-unloading ships. A method of a folding conveying boom with hydraulic-four-bar mechanisms was presented, and the size and motion of the four-bar mechanism were optimized with multiple objectives. The real connecting rod mechanism was manufactured and the folding conveyance equipment was developed. By looking at the practical applications, the developed folding conveying equipment had the advantages of smooth movement and high folding efficiency, which solved problems such as being unable to close and release the over-long and heavy-load conveying boom, a low efficiency and poor security at the source.

Competing interests

The authors declare that they have no competing interests.

Funding Information

The research was supported by the National Natural Science Foundation of China (No. 52175003, 51705034), the Natural Science Foundation of Hunan province (No. 2021JJ30726, 2021JJ40259), the Training Program for Excellent Young Innovators of Changsha (KQ2009053).

Author contributions

Juan Huang proposed the idea and conduct the research; Chongxiang Li derived the equations; Long Huang proposed the methodology; Lairong Yin participated in the scheme design; Bo Wen and Jinhang Wang participated in the design and manufacture of the folding mechanism.

References

- [1] L. Yin, J. Huang, L. Hu, X. Liu, Z. Zhang, A kind of dragon door conveyor. China, ZL201410640779.3, Invention patent, Date of authorization: 2016-9-14
- [2] M. Snowdon, M. Abdelwahab et al., Mechanical optimization of virgin and recycled poly(ethylene terephthalate) biocomposites with sustainable biocarbon through a factorial design, *Results Mater.* **5**, 100060 (2020)
- [3] Z. Qu, L. Yao et al., Rational design of HSNs/VO₂ bilayer coatings with optimized optical performances and mechanical robustness for smart windows, *Solar Energy Mater. Solar Cells* **200**, 109920 (2019)
- [4] M.E. Lynch, M. Mordasky, L. Cheng, A. To, Design, testing, and mechanical behavior of additively manufactured casing with optimized lattice structure, *Addit. Manufactur.* **22**, 462–471 (2018)
- [5] S.-G. Ye, J.-H. Zhang, B. Xu, Noise reduction of an axial piston pump by valve plate optimization, *Chin. J. Mech. Eng.* **31**, 57 (2018)

- [6] A. Hassan, M. Abomoharam, Modeling and design optimization of a robot gripper mechanism, *Robotics Comput. Integr. Manufactur.* **46**, 94–103 (2017)
- [7] W. Qiu, F. Lu, G. Wang et al., Evaluation of mechanical performance and optimization design for lattice girders, *Tunnel. Underground Space Technol.* **87**, 100–111 (2019)
- [8] Y. Yalcin, M. Orhon, O. Pekcan, An automated approach for the design of mechanically stabilized earth walls incorporating metaheuristic optimization algorithms, *Appl. Soft Comput.* **74**, 547–566 (2019)
- [9] R.V. Rao, R.B. Pawar, Constrained design optimization of selected mechanical system components using Rao algorithms, *Appl. Soft Comput.* **89**, 106141 (2020)
- [10] Z.F. Bai, J.J. Zhao, J. Chen, Y. Zhao, Design optimization of dual-axis driving mechanism for satellite antenna with two planar revolute clearance joints, *Acta Astronaut.* **144**, 80–89 (2018)
- [11] C.R. de Lima, G.H. Paulino, Auxetic structure design using compliant mechanisms: a topology optimization approach with polygonal finite elements, *Adv. Eng. Softw.* **129**, 69–80 (2019)
- [12] L.-Q. Wang, Z.-L. Wei, S.-M. Yao, Y. Guan, S.-K. Li, Sealing performance and optimization of a subsea pipeline mechanical connector, *Chin. J. Mech. Eng.* **31**, 18 (2018)
- [13] Y.-L. Ma, J.-R. Tan, D.-L. Wang, Z.-Z. Liu, Light-weight design method for force-performance-structure of complex structural part based co-operative optimization, *Chin. J. Mech. Eng.* **31**, 42 (2018)
- [14] Y. Lairong, H. Long, H. Juan, Solution-region-based synthesis approach for selecting optimal four-bar linkages with the Ball–Burmester point, *Mech. Sci.* **10**, 25–33 (2019)
- [15] L. Huang, L. Yin, B. Liu, Y. Yang, Design and error evaluation of planar 2-DOF remote center of motion mechanisms with cable transmissions, *ASME-J. Mech. Des.* **143**, 013301 (2021)
- [16] X. Zhang, J. Lu, Y. Shen, Simultaneous optimal structure and control design of flexible linkage mechanism for noise attenuation, *J. Sound Vibr.* **299**, 1124–1133 (2007)
- [17] P. Kuresangsai, M.O.T. Colea, Kinematic modeling and design optimization of flexure-jointed planar mechanisms using polynomial bases for flexure curvature, *Mech. Mach. Theory. Mechanism and Machine Theory*, **132**, 80–97 (2019)
- [18] W. Yea, X. Chai, K. Zhang, Kinematic modeling and optimization of a new reconfigurable parallel mechanism, *Mech. Mach. Theory* **149**, 103850 (2020)
- [19] M. Gabardi, M. Solazzi, A. Frisoli, An optimization procedure based on kinematics analysis for the design parameters of a 4-UPU parallel manipulator, *Mech. Mach. Theory* **133**, 211–228 (2019)
- [20] S. Nisar, T. Endo, F. Matsuno, Design and optimization of a 2-degree-of-freedom planar remote center of motion mechanism for surgical manipulators with smaller footprint, *Mech. Mach. Theory* **129**, 148–161 (2018)
- [21] M. Russo, S. Herrero, O. Altuzarra, M. Ceccarelli, Kinematic analysis and multi-objective optimization of a 3-UPR parallel mechanism for a robotic leg, *Mech. Mach. Theory* **120**, 192–202 (2018)
- [22] B. Hu, C. Zhou, H. Wang, L. Yin, Prediction and validation of dynamic characteristics of a valve train system with flexible components and gyroscopic effect, *Mech. Mach. Theory* **157**, 104222 (2021)
- [23] B. Hu, C. Zhou, H. Wang, S. Chen, Nonlinear tribo-dynamic model and experimental verification of a spur gear drive under loss-of-lubrication condition, *Mech. Syst. Signal Process.* **153**, 107509 (2021)

Cite this article as: J. Huang, C. Li, L. Huang, L. Yin, B. Wen, J. Wang, Multi-objective optimization design of a heavy-duty folding mechanism and Self-discharging equipment development, *Mechanics & Industry* **24**, 19 (2023)